Szpunar, I.; Wachowski, S.; Miruszewski, T.; Dzierzgowski, K.; Gornicka, K.; Klimczuk, T.; Sorby, M.... (2020). Electric and magnetic properties of Lanthanum Barium Cobaltite. Journal of the American Ceramic Society. 103(3):1809-1818. https://doi.org/10.1111/jace.16865

Electric and magnetic properties of Lanthanum Barium Cobaltite

Iga Szpunar[1], Sebastian Wachowski[1], Tadeusz Miruszewski[1], Kacper Dzierzgowski[1], Karolina Górnicka[1], Tomasz Klimczuk[1], Magnus Helgerud Sørby[2], María Balaguer[3], José M Serra[3], Ragnar Strandbakke[3], Maria Gazda[1], Aleksandra Mielewczyk-Gryń[1]

[1] Department of Solid State Physics, Faculty of Applied Physics and Mathematics, Poland

[2] Institute for Energy Technology, Department for Neutron Materials Characterization, P.O. Box 40, 2027 Kjeller, Norway

[3]Instituto de Tecnología Química (Universidad Politécnica de Valencia – Consejo Superior de Investigaciones Científicas), av. Los Naranjos s/n, E-46022 Valencia, Spain.

[4] Department of Chemistry, Centre for Materials Science and Nanotechnology, University of Oslo, FERMiO, Gaustadalléen 21, NO-0349 Oslo, Norway

Abstract

The cubic $Ba_{0.5}La_{0.5}CoO_{3-\delta}$ was synthesized using solid state reaction. The structural properties were determined by the simultaneous refinement of Synchrotron Powder X-ray Diffraction and Neutron Powder Diffraction data. Iodometric Titration was used to examine the oxygen stoichiometry and average cobalt oxidation state. Low-temperature magnetic studies show soft ferromagnetic character of fully oxidized material, with θ_P = 198(3) K and μ_{eff}=2.11(2) μ_B. Electric measurements show the thermally activated

nature of conductivity at low temperatures, whereas, due to the variable oxidation and spin state of cobalt, a single charge transport mechanism cannot be distinguished. Around room temperature a wide transition from thermally activated conductivity to semi-metallic behavior is observed. Under the inert atmosphere, the oxygen content lowers and the cation ordering takes place, leading to coexistence of two, ordered and disordered, phases. As a result of this change, thermally activated conductivity is observed also at high temperatures in inert atmosphere.

Introduction

The perovskite cobaltites, with a general formula $Ba_{0.5}Ln_{0.5}CoO_3$ (where Ln stands for rare earth metal), have gained much attention due to their electric and magnetic properties (1–3). In this group of materials the metal-insulator transition was observed, as well as high ionic conductivity (3). Additionally, the spin configuration of cobalt may vary for this system causing the antiferromagnetic (4), ferromagnetic (5) and even spin glass behavior (6). Moreover, high-temperature electrical properties $Ba_{0.5}La_{0.5}CoO_3$ (BLC) have been intensively studied for their potential application as electrode material for intermediate temperature solid oxide fuel cells and electrolyzers (IT-SOFC / -SOEC)(7,8).

Lanthanum barium cobaltites(2,9) crystallize in two crystal structures, i.e. disordered cubic ($Ba_{1-x}La_xCoO_{3-\delta}$), and ordered tetragonal ($BaLaCo_2O_6$)(2,6,10). In the cubic phase,

La and Ba cations occupy the same perovskite A-site, while in the tetragonal polymorph, divalent barium and trivalent lanthanum cations form alternating layers of [Co-O]/[Ba-O]/[Co-O]/[La-O] along the c-axis. The A-site cation ordering phenomena is a result of the difference between Ba and La ionic radii and occurs only for $x \geq 0.35$(6).

Cobalt exhibits different oxidation states (Co^{2+}, Co^{3+}, Co^{4+}) stable in the perovskite structure both in pyramidal and octahedral coordination(11–13). Moreover, the spin state of cobalt (3+ and 4+) changes with temperature, due to competing phenomena such as crystal field splitting (Δ_C), and the exchange interaction (Δ_E) of occupied orbitals and 3d electrons. With increasing temperature, the favorable spin state changes from the low spin state, through intermediate to high spin state(12,14). The mixed-valence of cobalt is connected to changes in oxygen stoichiometry of BLC, strongly affecting the electrical conductivity of the material(2,4,9). Oxygen stoichiometry can be controlled by modifying processing parameters, e.g. temperature and pO_2(9).

In the present work, the structural, electrical, and low-temperature magnetic properties of cubic BLC were examined. The electrical conductivity was measured in both low (2 K – RT) and high (RT – 800 K) temperature and under oxidizing and inert atmospheres. The change of oxygen non-stoichiometry has been analyzed in the wide temperature range while the atmosphere has been switched from oxidizing to inert. The work aims at establishing a relationship between the changes in Co spin and oxidation states,

electrical conductivity, and magnetic behavior. Barium lanthanum cobaltite perovskite have been investigated by structural, electrical and thermal methods yielding a broad landscape of its properties.

Experimental

$Ba_{0.5}La_{0.5}CoO_{3-\delta}$ was synthesized by solid-state reaction. Stoichiometric amounts of La_2O_3 (99.99% Alfa Aesar, preheated at 900 °C for 5 h), $BaCO_3$ (99.9% Sigma Aldrich) and Co_3O_4 (99.98% Alfa Aesar) were hand mixed and ground in an agate mortar with isopropyl alcohol as a medium, pelletized and annealed at 1150°C for 48 h in ambient air atmosphere.

The phase composition was characterized by X-ray powder diffraction method (Phillips X'Pert Pro) with Cu K_α radiation. Synchrotron Radiation Powder X-ray Diffraction (SR-PXD) patterns were obtained at the Swiss-Norwegian Beamlines (SNBL, BM01), ESRF, Grenoble with a Pilatus 2M 2-dimensional detector and a wavelength of 0.78956 Å. The samples were contained in 0.3 mm borosilicate capillaries that were rotated 90˚ during the 10 s exposure. The sample-detector distance was 138.2 mm. 1D data were obtained by integration of the 2D diffraction patterns using the program Bubble(15). Powder Neutron Diffraction (PND) data were collected at room temperature using the PUS diffractometer (λ =1.555 Å) at the JEEP II reactor (Kjeller, Norway)(16). The sample was loaded in vanadium can with 6 mm diameter. The results were analyzed using the

Rietveld method(17) with the Topas software from Bruker-AXS. The peak shapes were described by Thomson-Cox-Hasting split pseudo-Voigt fucntions with ten refinable parameters. The backgrounds were modeled with 6^{th} order (PND) and 12^{th} order (SR-PXD) Chebyshev polynomials. The structure model was refined simultaneously using the PND and SR-PXD data. The displacement parameters (B_{iso}) used to fit the SR-PXD pattern were allowed to differ from those refined from the PND data since they correlated strongly with the X-ray absorption.

Cobalt oxidation state and oxygen stoichiometry was determined by means of iodometric titration at room temperature. For this purpose, 15-20 mg of the sample and an excess of potassium iodide (ca. 0.2 g) were placed in a three-neck flask. To remove air from the flask and keep inert conditions during the whole measurement, nitrogen was continuously flowed through. After that, 15 ml of 2M HCl was added to dissolve the sample. The iodine ions were titrated using an aqueous solution of 0.01 mol/dm^3 $Na_2S_2O_3$ in a 10 ml microburet (±0.05 ml) while starch was used as indicator.

Micromeritics system was used to carry out a Temperature-Programmed Reduction (TPR). 100 mg of the solid sample was degassed under Ar flow for 1 h and then subjected to reduction under H_2/Ar (1/9 vol/vol) flow (50 ml/min), and heating rate of 10°C/min till 950°C. The H_2 consumption was measured by a Thermal Conductivity

Detector (TCD). The temperature dependence of the electrical resistivity was studied from 2 K to 1073 K.

The high-temperature (between RT and 1073 K) measurements were carried out with DC 4-point probe method using KEYSIGHT 34970A under synthetic air and argon. DC conductivity was recorded on a rectangular sample with a relative density of 77% and geometry of 2.45 x 1.05 x 4.5 mm^3 during the heating from RT to 800°C in air. Next, the atmosphere was changed from air to Ar and the sample was left to equilibrate in Ar for 13 hrs at 800°C. The voltage drop under 50 mA DC current was monitored during the equilibration process to reveal reduction kinetics through the change in electrical conductivity. Conductivity in Ar was measured during cooling after reaching equilibrium at 800°C.

The thermogravimetry (TGA) has been performed using Netzsch TG 209 F3 Tarsus thermobalance. The baseline for buoyancy correction was collected before the experiment by running a blank curve on empty alumina crucible. The measurements have been performed in tank dry purge gas (air upon heating and argon upon cooling) with heating/cooling rate of 2K/min. The starting point for cobalt oxidation state has been determined via iodometric titration as described previously.

Low-temperature measurements of resistivity were performed with a Quantum Design Physical Property Measurements System (PPMS). The resistivity was determined using a

standard four-probe technique, with four 37 μm diameter platinum wire leads spark-welded to the flat polished sample surface. The measurements were carried out between 2 K and 300 K under zero magnetic field. PPMS (with an AC susceptometer) was also used to measure the temperature-dependent magnetization. The measurements were performed in the temperature range of 2–300 K, in FC and ZFC mode, under an applied magnetic field of 0.5 T.

Results and discussion

Figure 1 presents the ND and SR-PXD patterns of BLC. The simultaneous Rietveld refinement of the PND and SR-PXD data confirmed the cubic structure (space group no. 221 Pm-3m) with a unit cell parameter of 3.8845(1) Å. A few minor peaks from an additional cubic phase are visible, and are fitted by a second cubic perovskite phase with the same composition as the main phase but with a = 3.9959(7) Å. The refined content of the secondary phase is 2.6(3) wt%. The structural data for the investigated sample are summarized in Table 1. The refined occupancy of the oxygen site is unity with a standard deviation of 0.007, giving an average cobalt valence state of +3.5. The result is consistent with the iodometric titration studies, in which the cobalt oxidation state has been determined as 3.42(9). The oxygen non-stoichiometry calculated from this value gives δ = 0.042(4). On the other hand, the thermally-programmed reduction study showed that the average oxidation state of cobalt is 3.95(1), which is equivalent to δ=-

0.225. Both titration and TPR studies have been repeated several times yielding reproducible values. The results suggest that H_2-based TPR is not suitable to investigate this composition and iodometric titration results should be used as the value of the averaged oxidation state of Co in the system.

Analysis of the electrical and magnetic properties requires consideration of at least three degrees of freedom for Co ions: oxidation state, coordination, and spin state. Based on the titration results and refinements of the neutron diffraction data, we consider a fully-oxidized system with half the Co ions in +3 and half in +4 oxidation states. The concentration of oxygen vacancies at room temperature is thus minuscule, and Co ions are located in oxygen octahedra. Thus, the number of Co ions coordinated pyramidally by five oxide ions is expected to be negligible at room temperature. The 3d electrons of Co in oxidation state 3+ or 4+ can be in high spin (HS), intermediate spin (IS), or low spin (LS) configuration, depending on temperature and degree of crystal field splitting (Figure 2)(1).

Temperature dependence of magnetic susceptibility as well as electrical conductivity was measured to determine the effect of spin transitions on conduction mechanisms. Figure 3a depicts the zero-field-cooled (ZFC) and field-cooled (FC) magnetization (M) as a function of temperature under an applied magnetic field of 0.5 T. Below 200 K a strong increase of magnetization is observed with decreasing temperature, indicating the

transition from para- to ferromagnetic state. The reciprocal magnetic susceptibility χ^{-1}(T) (where χ is defined as dM/dH, where M is the magnetization and H is the applied magnetic field) presented in the inset of Figure 3a, was used to calculate the transition temperature and the effective magnetic moment μ_{eff}. Between 225 and 300 K, the experimental data were fitted to the modified Curie-Weiss law (R^2 = 0.99), $\chi = C/(T-\theta_P)$, where C and θ_P are the Curie constant and the paramagnetic (PM) Curie temperature, respectively. The fit, shown by the red solid line in Figure 3a (inset) gave C = 1.67(2) emu K and θ_P = 198(3) K, whereas the derivative of the temperature dependence of magnetization shows the minimum at 180 K (not shown here). The obtained value is in good agreement with the data published previously(2). Also, Fauth et al. reported the transition between para- and ferromagnetic state in the stoichiometric BLC at 180 K (18). Moreover, they also observed the onset of the structural transition from cubic to tetragonal below 180 K. From C, the effective magnetic moment μ_{eff}, was calculated using the following relation:

$$\mu_{eff} = \sqrt{\frac{3Ck_B}{{\mu_B}^2 N_A}}, \qquad (1)$$

where k_B stands for Boltzmann constant, μ_B is Bohr magneton, and N_A is Avogadro constant. The effective moment determined from the Curie constant, μ_{eff} =2.11(2) μ_B, is comparable with the values reported elsewhere(2). The effective magnetic moment 2.11(2) μ_B is related to the spin state configurations of cobalt. Knowing that the average

cobalt oxidation state is +3.5 in BLC, the μ_{eff} value denotes the mixed-spin states of the cobalt ions. At temperatures below RT, low-spin states are preferable but μ_{eff} calculated for both Co^{3+} and Co^{4+} in low-spin configuration is 0.87 μ_B, which is significantly lower than the measured value. Possible spin states of cobalt ions in perovskite cobaltites have been studied for many years [see the references in (19)]. In view of these reports, the model postulating the presence of Co^{3+} and Co^{4+} in both LS and IS states may explain the effective moment. However, it should be taken into consideration that the presence of Co^{3+} and Co^{4+} in both low- and intermediate-spin states introduce lattice strain. The ionic radius of IS Co^{3+} is 0.56 Å (20) whereas the radius of IS Co^{4+} may be expected to be lower. On the other hand, it is known that BLC may undergo a transition from a disordered cubic perovskite into a B-site charge-ordered tetragonal structure. The phase transition is driven by the Jahn-Teller distortion of the CoO_6 octahedra, which is required for the intermediate spin state (21). Nakajima et al. reported that BLC undergoes the charge-ordering phase transition at 140 K (2), whereas Fauth et al. reported transition at 180 K (18). IS state of cobalt ions was reported in several cobaltites. Nakajima et al. (2) and Fauth et al. (18) explained the properties of BLC with the presence of IS state, whereas Toulemonde et al. observed IS cobalt state in strontium-doped lanthanum cobaltite (22).

Figure 3a shows that below 40 K the magnetization curves obtained in the FC and ZFC modes diverge. Several perovskite cobaltites show differences between ZFC and FC

curves below the Curie temperature. In particular, for measurements carried out in the low magnetic field, ZFC temperature dependence of magnetization may exhibit a maximum below Tc, whereas the magnetization decreases to a very low value with decreasing temperature, e.g. (23). Kumar and Banerjee showed that the difference between the FC and ZFC curves decreases with increasing field and at 1 T the FC and ZFC curves almost coincide (24). Such a characteristic is observed in our work since the magnetic field of 1 T was applied. In Figure 3b, we show the electrical resistivity in the same temperature range, showing no apparent effect of phase transition on the conductivity.

Figure 4 presents field dependence of isothermal magnetization in the paramagnetic regime at 250 K and below the transition temperature at 10 K. The coercive field, H_c, at 10 K is 1.35(10) kOe. The low value of H_c and low residual to saturation magnetization ratio indicates the nature of a soft ferromagnetic material. Above the transition temperature, hysteresis is not observed.

Temperature dependence of resistivity is shown in Figure 5. In the temperature range from 2 K to room temperature (Figure 5a), resistivity decreases with increasing temperature, changing the slope of the resistance curve, whereas in the range of high temperatures (Figure 5b) it increases with increasing temperature. That means that a semiconductor-metal transition occurs at a temperature close to RT. There is significant

scatter in the reported temperatures at which the minimum of resistivity is observed. Some authors(2,5) observed the minimum of resistivity at 120 K-140 K which they interpreted as resulting from charge ordering transition. On the other hand, Rautama et al. observed this change in the conductivity as a function of T-slope corresponding to a semiconductor-metal transition at Tc, around 190 K (25). Differences in resistivity dependences may originate from different microstructure, oxygen stoichiometry or local spin ordering of the studied samples.

Electronic conductivity in BLC occurs through electron (hole) hopping between different cobalt sites(11). The temperature dependence of resistivity in these materials is a complex problem since the energies of different interactions are comparable with one another. The most relevant energy scales are the bandwidth and bandgap, the on-site Coulomb repulsion, the long-range Coulomb interaction, the magnetic exchange energy and the crystal-field splitting which determines the different spin states in this system. Moreover, in these materials, strong electron-phonon interaction, as well as electron scattering on charged point defects, may be expected. Therefore, in different temperature ranges different conductivity mechanisms may occur. In view of the qualitative analysis of the $\rho(T)$ plot and magnetic transition observed at 180 K- 200 K, we divided the discussion into three main temperature ranges, namely, below 40 K, between 40 K and 180 K and above room temperature.

In the lowest temperatures studied, between 2 K and 10 K, the resistivity approaches the finite (residual) value. This suggests that the charge transport is not thermally activated in this temperature range and the residual resistivity is observed. At temperatures above 10 K, the resistivity starts to decrease with increasing temperature so that a thermally-activated transport process begins to be dominant. Nevertheless, between 10 K and 40 K a continuous change of the $\rho(T^{-1})$ slope can be seen, suggesting that a single transport mechanism cannot be distinguished.

In the temperature range between 40 K and 180 K, four different models for describing the temperature dependence of resistivity were applied. These are models, where either $\rho T^{-1} \propto exp(T^{-1})$, $\rho \propto exp(T^{-1})$, Efros-Shklovskii-type (ES) hopping $\rho \propto \exp(T_{ES}/T)^{\frac{1}{2}})$ (26), or Mott's variable range hopping (VRH) $\rho \propto \exp\left((T_{VRH}/T)^{\frac{1}{4}}\right)$ (27). Figure 6 shows the plots of resistivity versus $T^{-1/n}$, where n is 1, 2 or 4. Curve in Figure 6a shows no linear dependency in the whole measured range of temperature, whereas in Figures 6b-6d the ranges in which the plot is linear are 85 K-150 K, 70 K- 156 K and 70 K – 160 K, respectively. As can be seen, none of the above models describe the resistivity properly in the whole measured temperature range (Figure 6). Figure 6a represents conductivity dominated by small polarons hopping in which $\rho T^{-1} \propto exp(T^{-1})$. There is no linear dependency in the $\rho T^{-1} \propto exp(T^{-1})$ the plot, thus this type of transport should not be taken into consideration at low temperatures. This is in

agreement with previous works since small polaron conductivity in barium doped lanthanum cobaltites may be expected in the paramagnetic state (28), which in the case of $Ba_{0.5}La_{0.5}CoO_3$ is attained above 180 K. The second model, in which $\rho \propto exp(T^{-1})$, shown in Figure 6b, typically represents resistivity dominated by thermal excitation of electrons from valence- to conduction band in conventional semiconductors. This model is not appropriate either. However, the charge carriers are generated through the band gap, the temperature dependence of mobility is different from that exhibited by semiconductors, due to magnetic scattering and electron correlations. Both hopping mechanisms, i.e. Efros-Shklovskii (ES) hopping (Figure 6c) and variable range hopping (Figure 6d) mechanisms, seem to be in better agreement with the measured resistivity. ES hopping occurs in the presence of Coulomb interactions between electrons, which is present in cobaltites. Characteristic temperature T_{ES} is equal to 120 K, which limits the applicability of this model to the temperatures below 120 K. Moreover, the standard deviation of the ρ ($T^{-1/2}$) is higher than that of ρ ($T^{-1/4}$) dependence, which describes the variable range hopping transport. VRH mechanism occurs when the electron hopping between the closest neighbors is not always the most favorable and transport, therefore, takes place between ions further away from each other (29). Coexistence of Co^{3+} and Co^{4+} at different spin states would promote the VRH mechanism due to the spin blockade between some states. In the cubic structure, cobalt ions at different oxidation states are randomly distributed in the crystal lattice, thus the distance between cations

between which electron transfer is blocked is not constant. The Variable Hopping Range model (VRH) describes resistivity with the relation $\rho_{VRH} = \rho_O exp\left((T_{VTH}/T)^{1/4}\right)$ and using the linear fit (Figure 6d) the T_{VRH} may be determined. Knowing the T_{VRH} temperature, the density of localized states at the Fermi level can be calculated, $k_b T_{VRH} \approx \frac{21}{\zeta^3 N(E_f)}$, where 21 is a numerical factor calculated for many systems (30), ζ is the decay length of the localized states at Fermi level, usually taken as unit cell parameter. The T_{VRH} temperature was determined as 2500 K, so the density of states was $N(E_F) \approx 1.7 \cdot 10^{24}\, eV^{-1}cm^{-3}$, which is higher than of typical oxides, but is consistent with the observed semi-metallic behaviour and low resistivity. The VRH model describes transport mechanism well between 50 – 140 K. Above 140 K, the temperature dependence of resistivity deviates from the VRH relation. That may be attributed to the charge ordering transition, reported before(2).

Between 180 K and room temperature, we observe that resistivity becomes nearly independent of the temperature. This is usually explained by the partial occupation of the e_g band by electrons coming from IS states, which results in a semi-metallic behaviour(31). As the temperature increases, more and more Co ions get excited to IS and HS states, which results in the formation of a conduction band and disfavors spin ordering and thus destroys ferromagnetism(1,32). Indeed, the resistivity in air above room temperature increases with increasing temperature (Figure 5b), suggesting a

metallic-like conductivity. The temperature dependence of resistivity differs from that of a conventional metal, that is, resistivity is not proportional to T but to its higher power (approximately 3.5). The reason for the stronger dependence of resistivity on temperature could be related to decreased mobility, trapping on charged point defects or reduction in charge carrier concentration.

Summing up, the electrical conductivity of BLC in the temperature range from 2 K to 1070 K is dominated by different transport mechanisms, schematically shown in Figure 7. At the lowest temperature, below 10 K, the residual resistivity is observed. Between 10 – 40 K the resistivity decreases with increasing temperature and, due to continuous change of slope, it cannot be ascribed to any particular model. Above this regime, the variable range hopping is a prevailing mechanism. Further temperature increase gives rise to cobalt at intermediate- and high-spin state population and another thermally-activation conductivity mechanism are observed between 140 K and room temperature.

Electrical conductivity from RT to 1073 K was measured in air (RT-1073 K) and Ar (pO_2 10^{-6} atm (1073 K – RT)) (Figure 8). Between 370 K and 1070 K semi-metal behavior is observed, which indicates high-spin states of cobalt dominance associated with conduction band filling. Conductivity and mass change were monitored at 1073 K upon switching from air to argon to study electrical behavior during the reduction process (Figure 8b). During the reduction, conductivity decreased in two steps, one fast (30

mins) and one slow (9 hrs). Similar behavior is observed in mass relaxation. With increasing temperature, and decreasing oxygen partial pressure the material is reduced, which results in increasing charge carrier concentration. After reaching equilibrium in Ar, conductivity was measured upon cooling from 1073 K to RT in Ar, revealing much lower values than upon heating in air. While the conductivity in air was semi-metallic above RT, the material shows thermally activated conductivity in a more reduced state under an inert atmosphere.

Figure 9 shows the XRD patterns of the sample before and after the reduction. The initially sharp, cubic reflections are widened and beginning to separate after reduction, indicating phase separation. Under an argon atmosphere, partial A-site ordering is observed as the tetragonal double perovskite structure of $BaLaCo_2O_6$ emerges(33–35). Therefore, two stages of the reduction process may be explained in the following way: The first stage changes only the oxygen stoichiometry, which leads to a change in oxygen coordination of Co from octahedral to square pyramidal, with the additional splitting of the Co 3d orbital energies; a decrease of d_{z2}, and an increase of d_{x2-y2}. As an effect, d_{z2} no longer forms an overlapping conduction band. In such a case instead of metallic conductivity, an activation-type of conductivity is observed stemming from hopping of t_{2g} electron holes between cobalt (10,36). The electrical conductivity results are in accordance with previous (9,10).

In the second step i.e. in the slow process ~~involves~~ a much smaller mass change is observed, therefore this process involves mostly cations ordering which leads to the formation of the double perovskite structure of $BaLaCo_2O_6$. The presence of this phase contributes to a decrease in conductivity.

Conclusions

$BaLaCoO_3$ adopts cubic structure with fully occupied oxygen positions at room temperature. The electrical and magnetic measurements showed the influence of cobalt spin states and oxidation state on the electrical properties. The low-temperature electrical and magnetic measurements (2K-RT) reflect the difference in cobalt spin states at different temperatures. At low temperatures, LS is preferable, while IS and HS states population increases with temperature, forming a conduction band by overlapping e_g levels. Therefore, metallic type conductivity can be observed above 370 K, when the concentration of IS or HS cobalt ions is high enough to form a conduction band. The electrical conductivity mechanism of BLC in the high-temperature range (RT-1073K) varies with the measurement atmosphere, changing from metallic-like behavior in air, to activated polaron hopping between reduced Co t_{2g}-states states in Ar. We suggest that the change from metallic to thermally activated conductivity is caused by

the change of local symmetry around Co ions induced by reduction, and leading to LS electron configuration due to crystal-field splitting.

Acknowledgments

The authors acknowledge the skillful assistance from the staff of the Swiss–Norwegian Beamline (SNBL), at the European Synchrotron Radiation Facility (ESRF), Grenoble, France. National science

The research has been supported by the National Science Centre Poland under m.ERA.net funding scheme (2016/22/Z/ST5/00691).

Funding from the Spanish Government (PCIN-2017-125, RTI2018-102161) is kindly acknowledged.

Financial and scientific contributions from the Research Council of Norway (Grant nº 272797 "GoPHy MiCO") through the M-ERA.NET Joint Call 2016.

References

1. Ivanova NB, Ovchinnikov SG, Korshunov MM, Eremin IM, Kazak N V. Specific features of spin, charge, and orbital ordering in cobaltites. Physics-Uspekhi. 2009;52(8):789–810.
2. Nakajima T, Ichihara M, Ueda Y. New A-site ordered perovskite cobaltite LaBaCo2O6: Synthesis, structure, physical property and cation order-disorder effect. J Phys Soc Japan. 2005;74(5):1572–7.
3. Strandbakke R, Cherepanov VA, Zuev AY, Tsvetkov DS, Argirusis C, Sourkouni G, et al. Gd-and Pr-based double perovskite cobaltites as oxygen electrodes for proton ceramic fuel cells and electrolyser cells. Solid State Ionics. 2015;278:120–32.
4. Frontera C, Caneiro A, Carrillo AE, Oró-Solé J, García-Muñoz JL. Tailoring oxygen

content on PrBaCo2O5+δ layered cobaltites. Chem Mater. 2005;17(22):5439–45.

5. Fauth F, Suard E, Caignaert V, Domengès B, Mirebeau I, Keller L. Interplay of structural, magnetic and transport properties in thelayered Co-based perovskite LnBaCo 2 O 5 (Ln = Tb, Dy, Ho). Eur Phys J B. 2001;21(2):163–74.

6. Luo W, Wang F. Powder X-ray diffraction and Rietveld analysis of La1−xBaxCoO3 (0<x≤0.5). Powder Diffr. 2006;21(04):304–6.

7. Pang S, Jiang X, Li X, Su Z, Xu H, Xu Q, et al. Characterization of cation-ordered perovskite oxide LaBaCo 2O5+δ as cathode of intermediate-temperature solid oxide fuel cells. Int J Hydrogen Energy. 2012;37(8):6836–43.

8. Pang S, Jiang X, Li X, Wang Q, Su Z. A comparative study of electrochemical performance of La0.5Ba0.5CoO3-δand La0.5Ba0.5CoO3-δ-Gd0.1Ce0.9O1.95cathodes. Int J Hydrogen Energy. 2012;37(3):2157–65.

9. Bernuy-Lopez C, Høydalsvik K, Einarsrud M-A, Grande T. Effect of A-Site Cation Ordering on Chemical Stability, Oxygen Stoichiometry and Electrical Conductivity in Layered LaBaCo2O5+ δ Double Perovskite. Materials (Basel). 2016;9(3):154.

10. Garcés D, Setevich CF, Caneiro A, Cuello GJ, Mogni L. Effect of cationic order-disorder on the transport properties of LaBaCo2O6-δ and La0.5Ba 0.5CoO3-δ perovskites. J Appl Crystallogr. 2014;47(1):325–34.

11. Pang SL, Jiang XN, Li XN, Wang Q, Zhang QY. Structural stability and high-temperature electrical properties of cation-ordered/disordered perovskite LaBaCoO. Mater Chem Phys. 2012;131(3):642–6.

12. Suard E, Fauth F, Caignaert V. Rhombohedral distortion in the new disordered LaBaCo2O6perovskite. Phys B Condens Matter. 2000;276–278:254–5.

13. Goupil G, Delahaye T, Sala B, Lefebvre Joud F, Gauthier G. Selection and study of basic layered cobaltites as mixed ionic–electronic conductors for proton conducting fuel cells. Solid State Ionics. 2014;263:15–22.

14. Masuda H, Fujita T, Miyashita T, Soda M, Yasui Y, Kobayashi Y, et al. Transport and Magnetic Properties of R_{1−<I>x</I>}A<I>_x</I>CoO₃ (R = La, Pr and Nd; A = Ba, Sr and Ca). J Phys Soc Japan. 2003;72(4):873–8.

15. Dyadkin V, Pattison P, Dmitriev V, Chernyshov D, IUCr. A new multipurpose diffractometer PILATUS@SNBL. J Synchrotron Radiat. 2016;23(3):825–9.

16. Hauback B, Fjellvåg H, Steinsvoll O, Johansson K, Buset OT, Jørgensen J. The high resolution Powder Neutron Diffractometer PUS at the JEEP II reactor at Kjeller in Norway. J Neutron Res. 2000;8(3):215–32.

17. Rietveld HM. A profile refinement method for nuclear and magnetic structures. J Appl Crystallogr. 1969;2(2):65–71.

18. Fauth F, Suard E, Caignaert V. Intermediate spin state of Co 3 + and Co 4 + ions in La 0.5 Ba 0.5 CoO 3 evidenced by Jahn-Teller distortions.

Phys Rev B. 2001;65(6):060401.

19. Raveau B, Seikh MM. Magnetic and Physical Properties of Cobalt Perovskites. Vol. 23, Handbook of Magnetic Materials. Elsevier; 2015. 161–289 p.

20. Radaelli PG, Cheong SW. Structural phenomena associated with the spin-state transition in (formula presented). Phys Rev B - Condens Matter Mater Phys. 2002;66(9):1–9.

21. Lamonova K V., Zhitlukhina ES, Babkin RY, Orel SM, Ovchinnikov SG, Pashkevich YG. Intermediate-spin state of a 3D ion in the octahedral environment and generalization of the Tanabe - Sugano diagrams. J Phys Chem A. 2011;115(46):13596–604.

22. Toulemonde O, N'Guyen N, Studer F, Traverse A. Spin State Transition in LaCoO3 with Temperature or Strontium Doping as Seen by XAS. J Solid State Chem. 2001 May;158(2):208–17.

23. Troyanchuk IO, Bushinsky M V., Sikolenko V V., Ritter C. Spin Crossover and Magnetic Properties of Ba-Substituted Cobaltites. J Exp Theor Phys. 2019;128(1):98–104.

24. Kumar D, Banerjee A. Coexistence of interacting ferromagnetic clusters and small antiferromagnetic clusters in La0.5Ba0.5CoO3. J Phys Condens Matter. 2013 [cited 2018;25(21):216005–9.

25. Rautama E-L, Boullay P, Kundu AK, Caignaert V, Pralong V, Karppinen M, et al. Cationic Ordering and Microstructural Effects in the Ferromagnetic Perovskite $La_{0.5}Ba_{0.5}CoO_3$: Impact upon Magnetotransport Properties. Chem Mater. 2008 20(8):2742–50.

26. Efros AL, Shklovskii BI. Coulomb gap and low temperature conductivity of disordered systems. J Phys C Solid State Phys. 1975;8(4).

27. Mott NF. Conduction in glasses containing transition metal ions. J Non Cryst Solids. 1968;1(1):1–17.

28. Phelan D, Yu J, Louca D. Jahn-Teller spin polarons in perovskite cobaltites. Phys Rev B. 2008 Sep;78(9):094108.

29. Fauth F, Suard E, Caignaert V, Domengès B, Mirebeau I, Keller L. Interplay of structural, magnetic and transport properties in thelayered Co-based perovskite LnBaCo 2 O 5 (Ln = Tb, Dy, Ho). Eur Phys J B. 2001;21(2):163–74.

30. Ambegaokar V, Halperin BI, Langer JS. Theory of hopping conductivity in disordered systems. J Non Cryst Solids. 1972;8–10(C):492–6.

31. Raveau B (Bernard), Seikh MM. Cobalt oxides : from crystal chemistry to physics. Wiley-VCH; 2012. 333 p.

32. Maria J, Nazir S, Alay-E-Abbas SM, Shaukat A. Half-metallic ferromagnetism in ordered LaBaCo2O6and disordered La0.5Ba0.5CoO3: DFT+U study. J Magn Magn Mater. 2014;368:230–3.

33. Malyshkin D, Novikov A, Tsvetkov D, Zuev A. Preparation, oxygen nonstoichiometry and defect structure of double perovskite LaBaCo2O6–δ. Mater Lett. 2018;229:324–6.

34. Malyshkin DA, Novikov AY, Sereda V V., Ivanov IL, Tsvetkov DS, Zuev AY. *In Situ* and *ex Situ* Study of Cubic La $_{0.5}$ Ba $_{0.5}$ CoO $_{3-\delta}$ to Double Perovskite LaBaCo $_{2}$ O $_{6-\delta}$ Transition and Formation of Domain Textured Phases with Fast Oxygen Exchange Capability. Inorg Chem. 2018;57(19):12409–16.

35. Bernuy-Lopez C, Rioja-Monllor L, Nakamura T, Ricote S, O'Hayre R, Amezawa K, et al. Effect of Cation Ordering on the Performance and Chemical Stability of Layered Double Perovskite Cathodes. Materials (Basel). 2018;11(2):196.

36. Bausá N, Solís C, Strandbakke R, Serra JM, Bausa Nuria, Solis Cecilia, Strandbakke Ragnar SJM, Bausá N, et al. Development of composite steam electrodes for electrolyzers based on barium zirconate. Solid State Ionics. 2017 Aug;306:62–8.

Figure Caption List

Figure 1 PND (a) SP-PXD (b) powder diffraction patterns of BLC fitted by Rietveld refinement. The wavelengths are 0.7896 Å and 1.5543 Å, respectively. Black points are experimental data, the solid profile is calculated from the refined model and the red line below is the difference plot. Vertical tick marks show Bragg peak positions.

Figure 2 Possible distributions of electrons in, a high spin (HS), intermediate spin (IS) or low spin (LS) state for cobalt 3+ and 4+.

Figure 3 Magnetic susceptibility as a function of temperature under field cooling (FC) and zero-field cooling (ZFC) mode (a) and temperature dependence of resistivity (b)

Figure 4 Field dependence of magnetization M(H) at 10 K (black) and 250 K (red)

Figure 5 Temperature dependence of resistivity in air frim 2 K to room temperature (a), and high temperature (b)

Figure 6 Low-temperature resistivity explained by the means of different transport models: small polaron hopping (a), thermally activated conductivity (b), Efros-Shklovskii mechanism (c), Variable range hopping (VRH) (d). The straight lines in red color represent the model fits and the black points are the data

Figure 7 Temperature dependence of predominant transport mechanism under air atmosphere

Figure 8 High-temperature resistivity in air and argon (a) and kinetics of sample reduction in argon at 800°C measured by the means of DC-4W electrical and thermogravimetric relaxation (b)

Figure 9 X-ray diffraction pattern of BLC before (black line) and after (red line) electrical measurements in Ar

Table Caption List

Table 1 Crystal structure of $Ba_{0.5}La_{0.5}CoO_6$ refined from PND and SR-PXD data.

Figure 1.

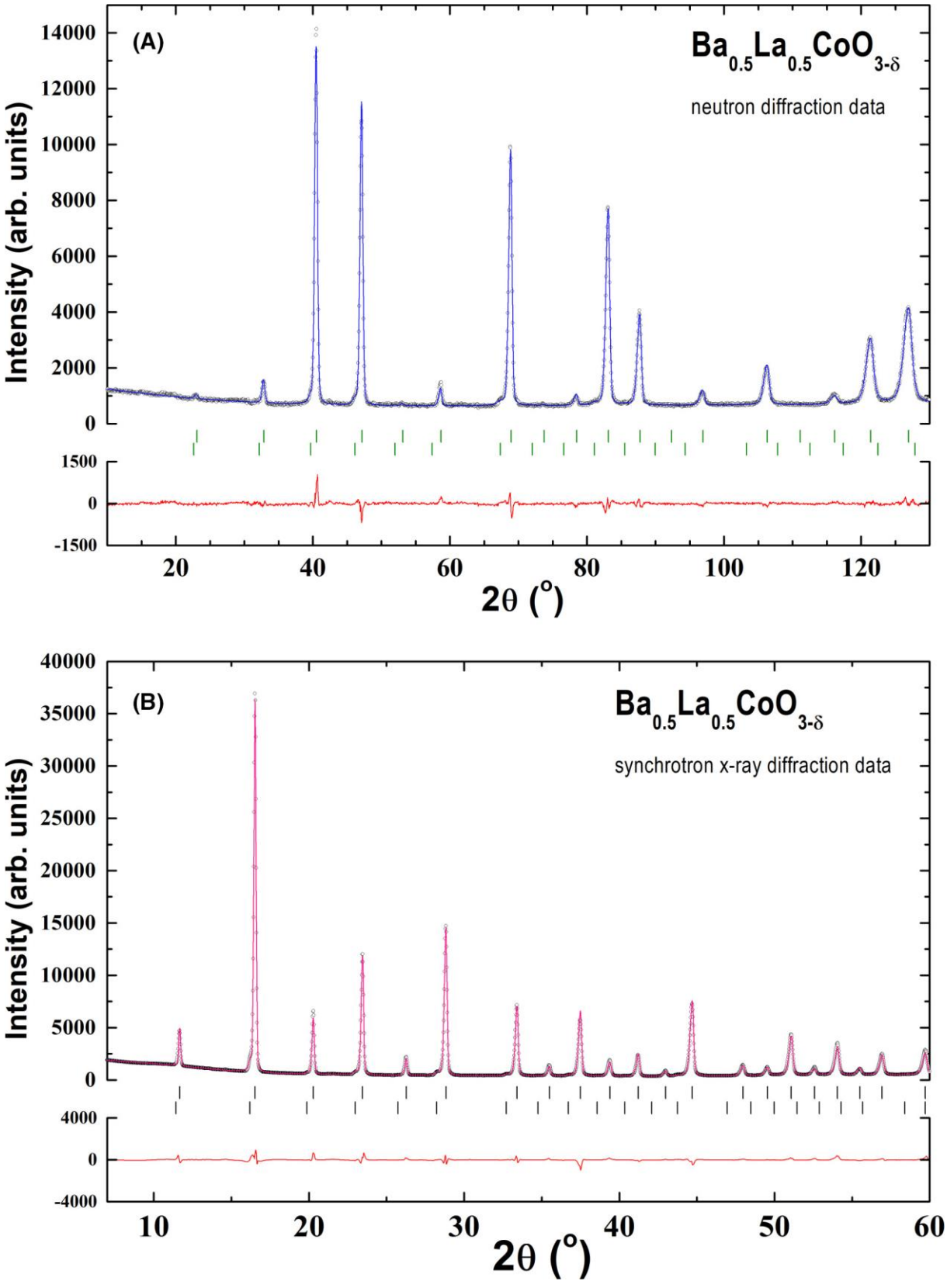
(A)
$Ba_{0.5}La_{0.5}CoO_{3-\delta}$
neutron diffraction data
Intensity (arb. units)
2θ (°)
(B)
$Ba_{0.5}La_{0.5}CoO_{3-\delta}$
synchrotron x-ray diffraction data
Intensity (arb. units)
2θ (°)

Figure 2

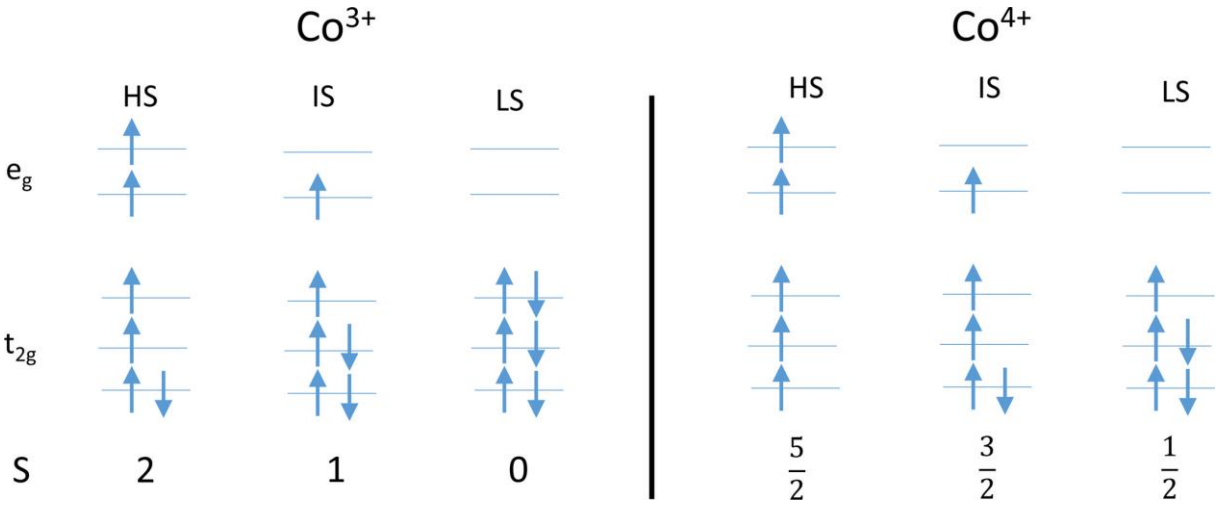

Figure 3

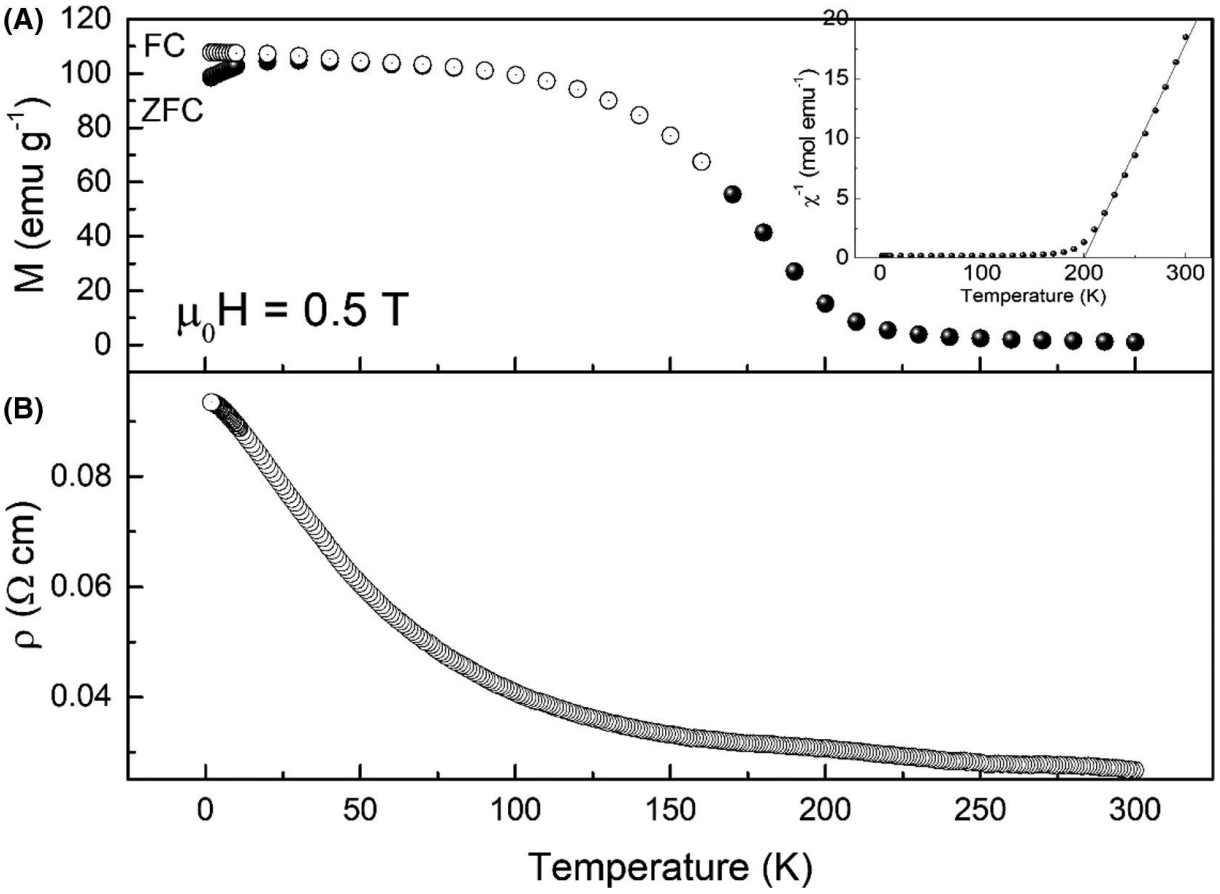

Figure 4

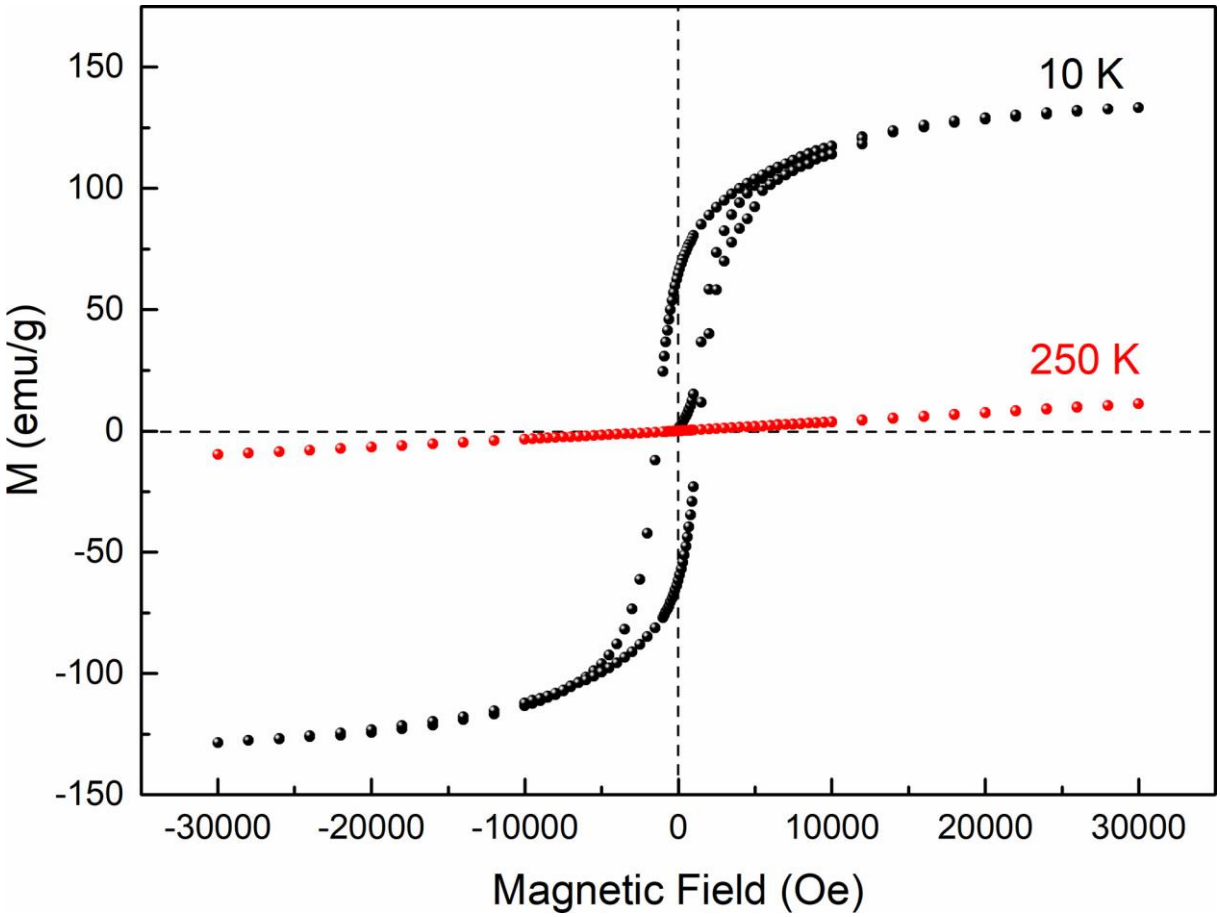

Figure 5

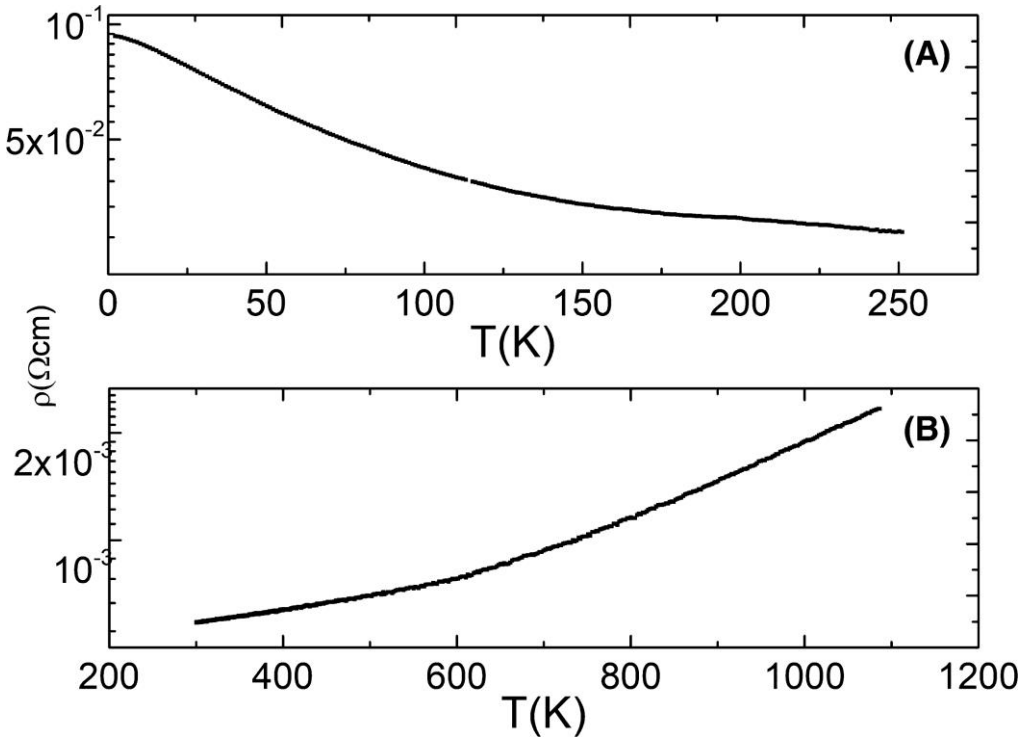

Figure 6

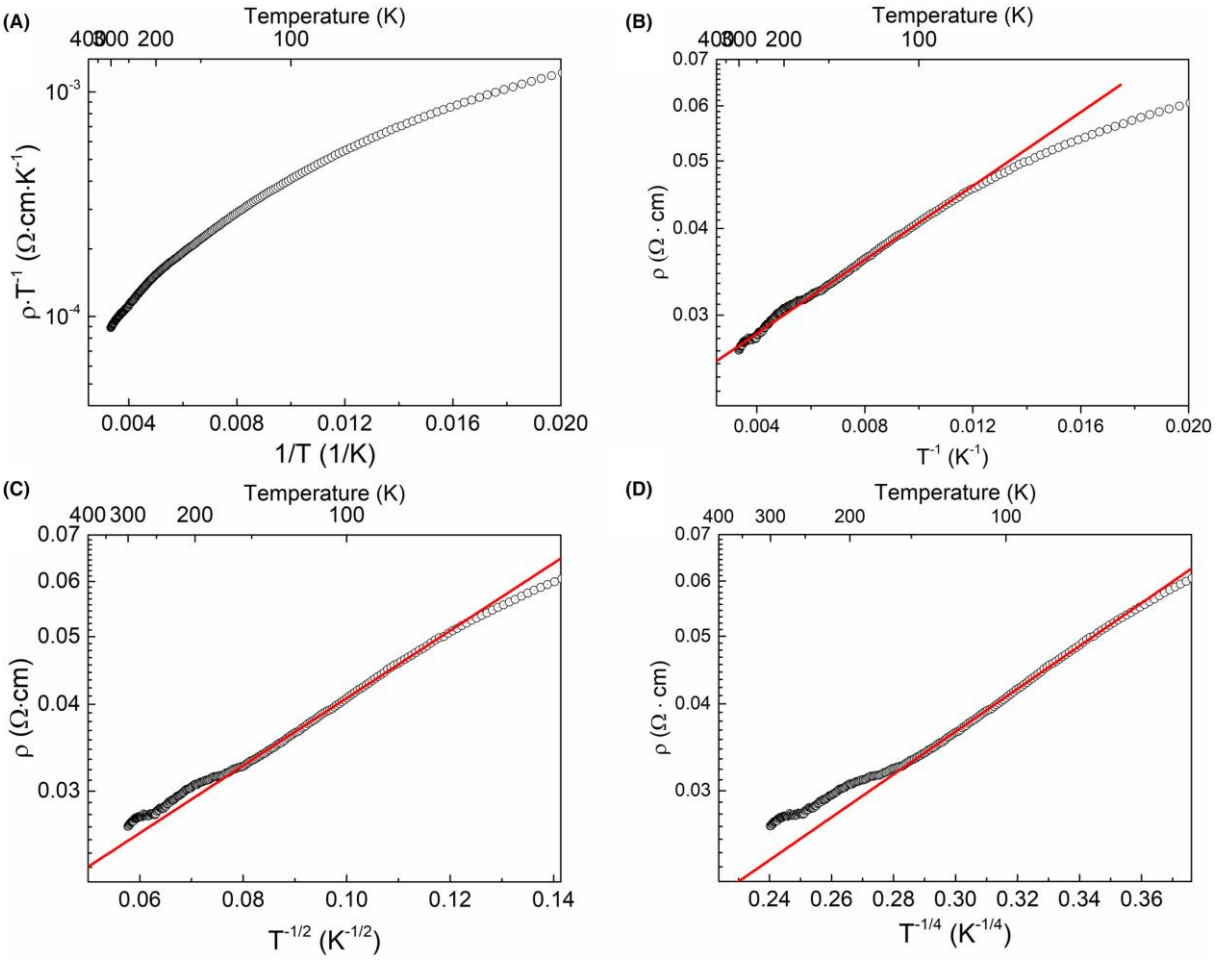

Figure 7

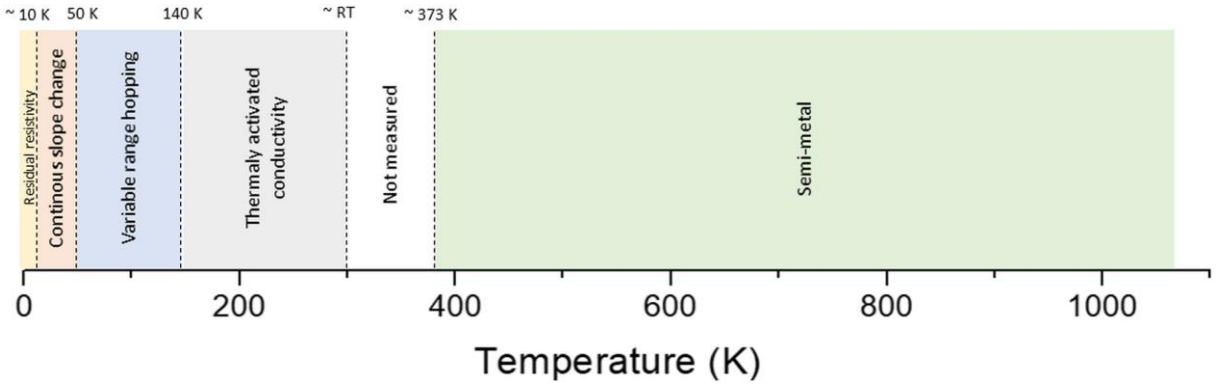

Figure 8

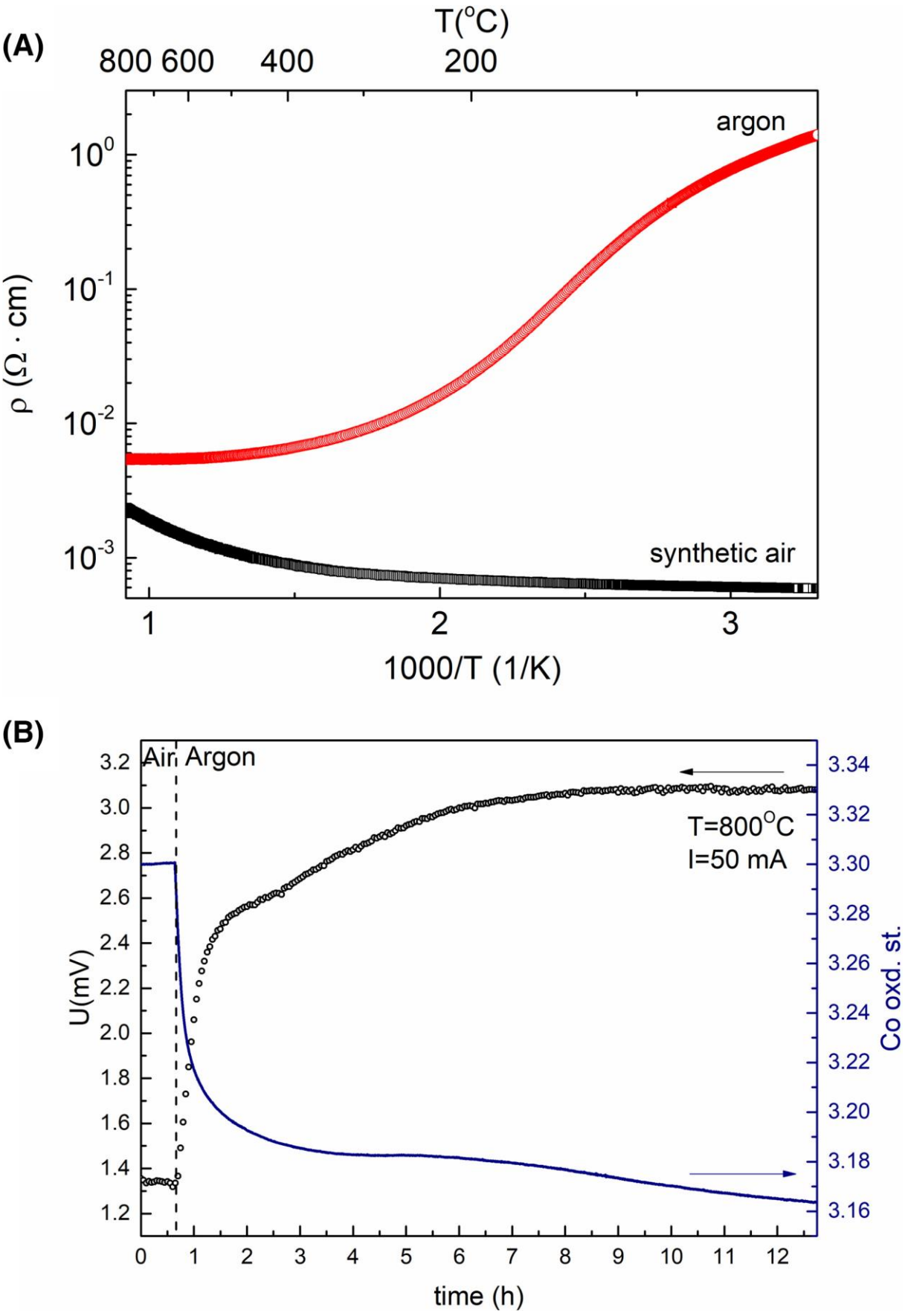
(A)
T(°C)
800 600
400
200
argon
synthetic air
ρ (Ω · cm)
10^0
10^-1
10^-2
10^-3
1
2
3
1000/T (1/K)
(B)
Air
Argon
T=800°C
I=50 mA
U(mV)
Co oxd. st.
time (h)

Figure 9

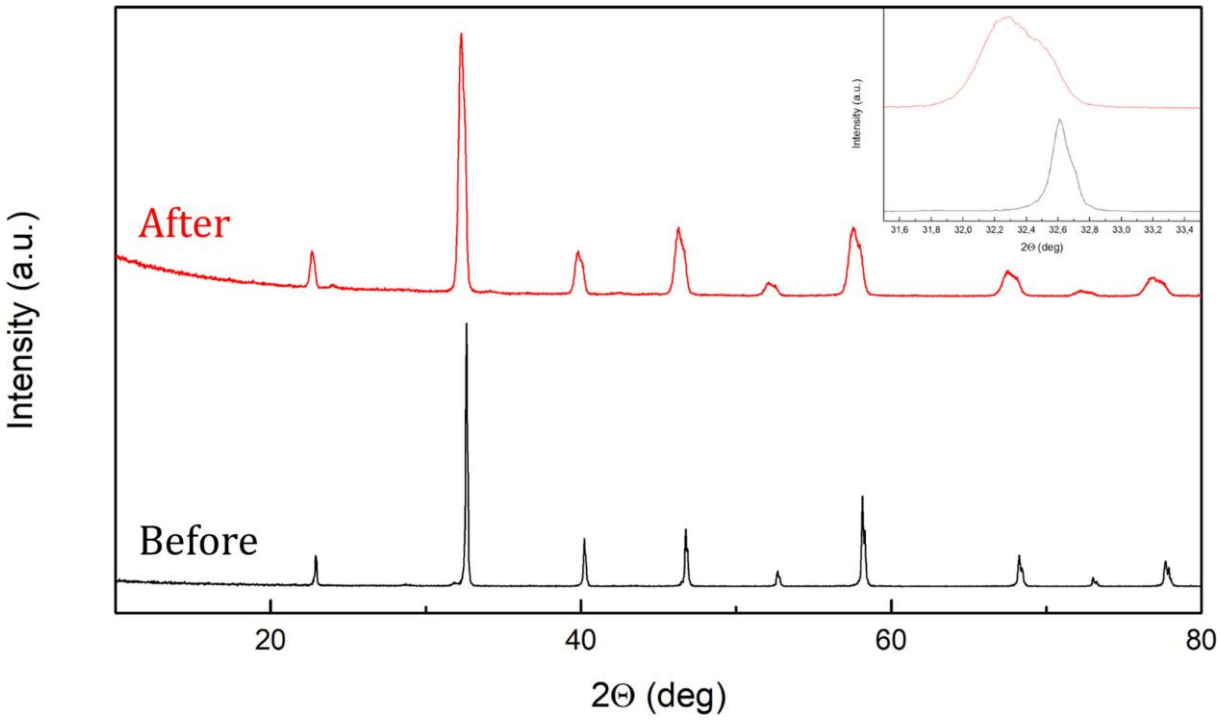
After
Before
Intensity (a.u.)
2Θ (deg)
20
40
60
80
Intensity (a.u.)
31,6
31,8
32,0
32,2
32,4
32,6
32,8
33,0
33,2
33,4
2Θ (deg)